AIAA JOURNAL
Vol. 42, No. 6, June 2004

Wall Function Boundary Conditions Including Heat Transfer and Compressibility

R. H. Nichols*
University of Alabama in Birmingham, Birmingham, Alabama 35294
and
C. C. Nelson†
Jacobs Sverdrup Arnold Engineering Development Center Group, Arnold Air Force Base, Tennessee 37389

Wall function boundary conditions that include the effects of compressibility and heat transfer are developed for transport-type turbulence models. The wall functions are based on coupled velocity and temperature profiles valid in both the viscous sublayer and the log layer. The wall function boundary conditions are developed within a rigid set of assumptions so that a consistent set of relationships are derived for the wall shear stress, the wall heat transfer, and the turbulence quantities at the first point off the wall. The new boundary conditions are incorporated into a Navier–Stokes computational fluid dynamics code that includes the Spalart–Allmaras and shear stress transport turbulence models. The wall function boundary conditions produce reasonable engineering solutions for the test cases presented for initial wall spacings of $y^+ \leq 100$.

Nomenclature

B	=	law-of-the-wall constant
C_f	=	skin friction
C_h	=	Stanton number
C_p	=	pressure coefficient
C_μ	=	two-equation turbulence model eddy-viscosity constant
C_{v1}	=	Spalart–Allmaras turbulence model constant
K	=	molecular thermal conductivity
K_t	=	turbulent thermal conductivity
k	=	turbulent kinetic energy
M	=	Mach number
P	=	pressure
Pr	=	molecular Prandtl number
P_t	=	total pressure
q_w	=	wall heat transfer
Re	=	Reynolds number
Re_x	=	Reynolds based on the distance from the leading edge of a plate
r	=	recovery factor, $Pr^{1/3}$
T	=	temperature
T_t	=	total temperature
T_w	=	wall temperature
u	=	velocity parallel to the wall
u_τ	=	friction velocity, $\sqrt{(\tau_w/\rho_w)}$
y	=	coordinate direction normal to the wall
ε	=	turbulent dissipation
κ	=	law-of-the-wall constant
μ	=	molecular viscosity
μ_t	=	eddy viscosity
μ_w	=	wall molecular viscosity
ρ	=	density
ρ_w	=	wall density
τ_w	=	wall shear stress
ω	=	specific turbulent dissipation

Received 2 July 2003; revision received 29 January 2004; accepted for publication 10 February 2004.

*Research Associate Professor, Department of Mechanical Engineering. Senior Member AIAA.
†Senior Engineer. Senior Member AIAA.

Introduction

TURBULENT transport models that are applicable all of the way to the wall are called low-Reynolds-number turbulence models because they are valid at low turbulent Reynolds numbers $[\rho k^2/(\mu\varepsilon)]$. Low-Reynolds-number models require tight grid spacing near the wall to resolve the large gradients in velocity, temperature, and turbulent quantities near the wall. This can lead to large grid requirements for three-dimensional Navier–Stokes applications. The stability of a numerical algorithm is limited by the smallest cell size in a grid, so that the small cells near the wall can severely restrict the maximum allowable time step for a problem. The near-wall turbulence damping terms are often expressed in terms of exponential functions. This can lead to difficulties in converging the numerical solution in the near-wall region.

Turbulence models that do not include wall correction terms in the differential equations are called high-Reynolds-number turbulence models. High-Reynolds-number turbulence models rely on empirically derived algebraic models of the near-wall region of the boundary layer to provide boundary condition information to the mean flow Navier–Stokes equations at the first point off the wall. These models of the near-wall region are called wall functions. Because the high-gradient region near the wall is modeled with these empirical relationships, the first point off the wall may be placed much farther away than with low-Reynolds-number models. This reduces the number of points required to discretize a flowfield and increases the maximum allowable time step. Both of these advantages are especially useful in modeling unsteady viscous flows.

Most of the early wall function boundary conditions were based on the analysis of Millikan[1] and Tennekes and Lumley[2] for channels and flat plates. Most of the early models did not include the effects of pressure gradient or heat transfer. Nichols,[3] Viegas et al.,[4] and Smith[5] have all developed wall functions that included heat transfer at the wall. These formulations were not based on a single unified velocity profile, so that the wall functions were often discontinuous in the transition region from the sublayer to the log layer. Wilcox[6] introduced a wall-matching methodology in which a set of differential equations were used to integrate from the wall to the first point off the wall. The wall-matching strategy requires a different set of differential equations for each different turbulence model. Frink[7] developed a set of wall functions for adiabatic walls based on the unified theory of Spalding.[8] Shih et al.[9] describe a unified wall function also based on Spalding's work, which includes pressure gradient effects but does not include coupling with heat transfer at the wall. This paper describes a wall function boundary condition based on coupled velocity and temperature boundary-layer profiles

that are applicable to incompressible flows, compressible flows, and flows with heat transfer. The wall function boundary conditions are developed within a rigid set of assumptions so that a consistent set of relationships are derived for the wall shear stress, wall heat transfer, and the turbulence quantities at the first point off the wall. This paper also describes the methodology for implementing the wall function boundary condition into a Navier–Stokes flow solver. The wall functions described here are compatible with most transport-type turbulence models.

Theory

There are six fundamental assumptions used in the development of wall function boundary conditions for compressible flows:

1) Analytical expressions are available for the velocity and temperature profiles in the lower part of the boundary layer.

2) Analytical expressions are available for the turbulent transport variables at the first point off the wall.

3) There is no pressure gradient normal to the wall in the lower part of the boundary layer.

4) The shear stress, $\tau_w = \tau = (\mu + \mu_t)(\partial u/\partial y)$, is constant in the lower part of the boundary layer.

5) The heat transfer, $q_w = q = (K + K_t)(\partial T/\partial y)$, is constant in the lower part of the boundary layer.

6) There are no chemical reactions, that is, the chemistry is frozen, in the lower part of the boundary layer.

Several empirical relationships are available for the velocity in a boundary layer that can be used to develop wall function boundary conditions. A typical boundary-layer velocity profile is shown in Fig. 1. The simplest form is the adiabatic incompressible universal law-of-the-wall

$$u^+ = (1/\kappa)\log(y^+) + B \tag{1}$$

where u^+ and y^+ are defined as

$$u^+ = u/u_\tau \tag{2}$$

$$y^+ = \rho_w u_\tau y/\mu_w \tag{3}$$

The universal law-of-the-wall is valid for the y^+ range of about $30 < y^+ < 1000$. The velocity in the sublayer, $0 < y^+ < 10$, is given by

$$u^+ = y^+ \tag{4}$$

The sublayer must be blended with the law-of-the-wall to cover the interim region. Spalding[8] suggested a unified form valid for the log layer and the sublayer as well as the transition region. This form is given by

$$y^+ = u^+ + e^{-\kappa B}\left[e^{\kappa u^+} - 1 - \kappa u^+ - (\kappa u^+)^2/2 - (\kappa u^+)^3/6\right] \tag{5}$$

Note that the $e^{-\kappa B}e^{\kappa u^+}$ term in Eq. (5) is a restatement of the incompressible adiabatic law-of-the-wall [Eq. (1)]. The constants κ and B are generally taken as 0.4 and 5.5, respectively. The wall function boundary condition can be tuned for such effects as surface roughness by adjusting the κ and B constants. Compressibility and heat transfer effects can be included by replacing the incompressible adiabatic law-of-the-wall term in Spalding's equation (5)

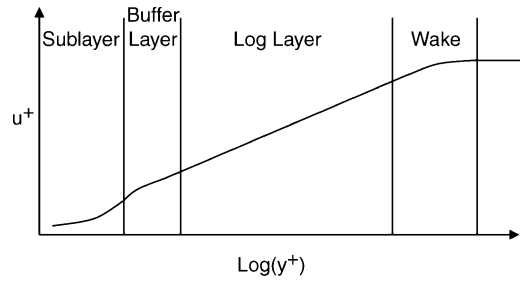

Fig. 1 Typical boundary layer profile.

with the outer velocity form of White and Christoph.[10] White and Christoph's outer velocity is given by

$$u^+ = (1/2\Gamma)\left\{\beta + Q\sin\left[\Phi + \left(\sqrt{\Gamma}/\kappa\right)\ell_n\left(y^+/y_0^+\right)\right]\right\} \tag{6}$$

where

$$\Gamma = \frac{r\,u_\tau^2}{2c_pT_w}, \qquad \beta = \frac{q_w\mu_w}{\rho_wT_wk_wu_\tau}, \qquad \varphi = \sin^{-1}\left(\frac{-\beta}{Q}\right)$$

$$Q = (\beta^2 + 4\Gamma)^{\frac{1}{2}}, \qquad y_0^+ = e^{-\kappa B} \tag{7}$$

The nondimensional parameter Γ models compressibility effects, and the parameter β models heat transfer effects. The wall shear stress τ_w appears in the definitions of u^+, y^+, Γ, and β. The wall heat transfer q_w appears only in the definition of β. The original formulation of the outer velocity also included a parameter for pressure gradient in Eq. (10). The pressure gradient parameter has been ignored in this effort because of the difficulty of determining a pressure gradient parameter for general three-dimensional flows. The outer velocity form of White and Christoph reduces to the standard law-of-the-wall [Eq. (1)] for incompressible adiabatic flow. Equation (5) can then be written as

$$y^+ = u^+ + y^+_{\text{White}} - e^{-\kappa B}[1 + \kappa u^+ + (\kappa u^+)^2/2 + (\kappa u^+)^3/6] \tag{8}$$

where

$$y^+_{\text{White}} = \exp\left(\left(\kappa/\sqrt{\Gamma}\right)\{\sin^{-1}[(2\Gamma u^+ - \beta)/Q] - \phi\}\right)e^{-\kappa B} \tag{9}$$

The temperature distribution within the boundary layer is given by the Crocco–Busemann equation[10]

$$T = T_w[1 + \beta u^+ - \Gamma(u^+)^2] \tag{10}$$

Hence, the boundary-layer profile is defined in terms of the shear stress τ_w and the wall heat transfer q_w. For adiabatic wall cases, $q_w = 0$, and the Crocco–Busemann equation reduces to

$$T = T_w\{1 + [(\gamma - 1)r/2]u^2\} \tag{11}$$

White and Christoph validated the ability of their outer law to predict skin friction with experimental data for 426 adiabatic wall cases and with 147 cold-wall cases in Ref. 10 and found that the absolute error $[(1/N)\sum|e_i|]$ was 5.17% for the adiabatic cases and 12.29% for the cold wall cases. The absolute error of their correlation was about the same as the best boundary-layer correlations of the time.

The wall shear stress for adiabatic flows is determined as follows:

1) Set the velocity at the wall to zero for nonmoving body problems or to the grid velocity for moving body problems.

2) Given the velocity and temperature at the first point off the wall; solve Eq. (11) for the wall temperature T_w.

3) Extrapolate the pressure from the first point off the wall and solve for the wall density ρ_w using the equation of state.

4) Iteratively solve Eq. (8) for the wall shear stress τ_w in the wall coordinate system given the distance of the first point off the wall from the wall.

5) Rotate the stress tensor into the computational coordinate system, and replace the viscous flux calculation at the wall for cell-centered algorithms or at the half-node for node-centered algorithms.

The wall shear stress and the heat transfer for constant temperature wall flows are determined as follows:

1) Set the velocity at the wall to zero for nonmoving body problems or to the grid velocity for moving body problems.

2) Extrapolate the pressure from the first point off the wall and solve for the wall density using the equation of state with the given wall temperature.

3) Iteratively solve Eqs. (8) and (10) for the wall shear stress τ_w and heat transfer q_w in the wall coordinate system given the distance of the first point off the wall from the wall.

4) Rotate the stress tensor and the heat transfer vector into the computational coordinate system, and replace the viscous flux calculation at the wall for cell-centered algorithms or at the half-node for node-centered algorithms.

One approach to introducing the wall function corrected wall shear stress and heat transfer into the calculation of the viscous fluxes has been to calculate an effective wall eddy viscosity so that the discrete shear stress at the first-half point off the wall given by

$$\tau_{1.5} = [(\mu_1 + \mu_2)/2 + (\mu_{t1} + \mu_{t2})/2][(u_2 - u_1)/(y_2 - y_1)] \quad (12)$$

yields the correct value for the wall shear stress. Unfortunately, this approach introduces errors into the energy equation because the slope of the temperature derivative will not be calculated correctly, that is, a separate effective wall eddy viscosity would be required for the temperature.

Sondak and Pletcher[11] describe a procedure to perform a transformation of the stresses for generalized coordinate systems. Although this transformation is much more general than the effective wall eddy-viscosity approach and introduces no error in the energy equation, it is also much more complex. In their transformation, the wall function-generated wall shear stress is assumed to be in the wall coordinate system, that is, a system aligned with velocity vector at the first point off the wall and the normal vector to the wall. This is not always the case for separated flows, but the assumption seems to produce reasonable results even when the flow is separated.

Another method of correcting the computational shear stress at the wall with the wall function value is to calculate the ratio of the magnitude of the computed wall shear stress to the wall function value and then scale the computed values by this ratio. This is equivalent to performing the transformation of Sondak and Pletcher[11] and is much simpler to apply. The temperature derivative at the wall may be treated in a similar manner.

Once the wall shear stress has been calculated, the turbulence transport variables must be determined at the first point off the wall. The eddy viscosity at the first point off the wall for incompressible adiabatic flow can be found using the constant stress assumption to be

$$\mu_t/\mu_w = \kappa e^{-\kappa B}\left[e^{\kappa u^+} - 1 - \kappa u^+ - (\kappa u^+)^2/2\right] \quad (13)$$

The equivalent form of the eddy viscosity for compressible flows with heat transfer can also be found using the constant stress assumption. The eddy viscosity is given by

$$\frac{\mu_t}{\mu_w} = 1 + \frac{\partial y^+_{\text{White}}}{\partial y^+} - \kappa e^{-\kappa B}\left(1 + \kappa u^+ + \frac{(\kappa u^+)^2}{2}\right) - \frac{\mu_{w+1}}{\mu_w} \quad (14)$$

where μ_{w+1} is the molecular viscosity at the first point off the wall and $\partial y^+_{\text{White}}/\partial y^+$ is given by

$$\frac{\partial y^+_{\text{White}}}{\partial y^+} = 2y^+_{\text{White}}\frac{\kappa\sqrt{\Gamma}}{Q}\left[1 - \frac{(2\Gamma u^+ - \beta)^2}{Q^2}\right]^{\frac{1}{2}} \quad (15)$$

Equation (14) reduces to Eq. (13) for adiabatic incompressible flows. This eddy-viscosity formulation provides a Wilcox[6]-like wall matching for the turbulence variables if the eddy viscosity is used to define the turbulence variable at the first point off the wall. This eddy-viscosity formulation is independent of the turbulence model chosen.

Turbulence Model Boundary Conditions

The values of the transport model turbulence variables at the first point off the wall must also be defined. The values for the Spalart–Allmaras[12] variable $\tilde{\nu}$ can be found by iteratively solving the following equation:

$$\tilde{\nu}^4 = \mu_t\tilde{\nu}^3 + \mu_t C^3_{v1} \quad (16)$$

The turbulent kinetic energy and turbulent dissipation at the first point off the wall for k–ε turbulence models are given by

$$k = u_\tau^2/\sqrt{C_\mu} \quad (17)$$

$$\varepsilon = C_\mu \rho k^2/\mu_t \quad (18)$$

The turbulent kinetic energy and specific turbulent dissipation at the first point off the wall for k–ω and shear stress transport (SST) turbulence models are given by

$$\omega_i = \frac{6\mu_w}{0.075\rho_w y^2} \quad (19)$$

$$\varpi_o = \frac{u_\tau}{\sqrt{C_\mu}\kappa y} \quad (20)$$

$$\varpi = \sqrt{\varpi_i^2 + \varpi_o^2} \quad (21)$$

$$k = \frac{\varpi\mu_t}{\rho} \quad (22)$$

The two-level model for ω in Eqs. (19–22) was suggested by Veiser et al.[13]

Additional Modifications to Flow Solvers for Wall Functions

Most upwind flow solvers require no further modifications than the inclusion of the corrected wall stress and heat transfer in the viscous flux calculations. The smoothers used with central difference algorithms require some additional modifications. The fourth-order smoother used to maintain numerical stability will produce excessive dissipation at the wall when wall functions are employed because of the large velocity difference between the wall and the first point off the wall. To prevent this from occurring, the smoother should be modified as follows. The standard form of the explicit fourth-order smoother in the ξ computational direction is

$$\Delta t\nabla_\xi\left[\psi^{(4)}\Delta_\xi\Lambda_\xi\right] \quad (23)$$

where

$$\Lambda_\xi = \nabla_\xi\Delta_\xi(J\boldsymbol{q})^{n+1}_j \quad (24)$$

where Δt is the time step, Δ_ξ is the central difference operator, and $\psi^{(4)}$ is the explicit fourth-order smoothing coefficient. The second derivative term Λ_ξ is normally set to zero at the wall for viscous calculations. This term is also set to zero at the first point off the wall when wall functions are used. This effectively turns the fourth-order smoothing off at the first point off the wall and reduces it significantly at the second point off the wall.

Once the wall shear stress is calculated using wall functions, the y^+ value of the first point off the wall is known. It is a simple matter to switch automatically between the wall functions and to integrate to the wall based on the local value of y^+. The turbulence model chosen should contain the low-Reynolds-number terms required for the model to be valid in the near-wall region if automatic switching is implemented. Automatic switching offers advantages in complex configurations because computational grid points can be saved by using the larger wall function wall spacings on nonessential portions of the geometry and integrating to the wall where high-quality skin friction or heat transfer is required. Automatic switching is also useful in grid sequencing or multigrid algorithms where the wall functions can provide an improved estimate of the wall shear stresses and heat transfer on the coarse mesh solutions.

Applications

The wall function boundary conditions described earlier were incorporated into the NXAIR[14] three-dimensional overset Navier–Stokes code. NXAIR is an implicit upwind Navier–Stokes code that employs a Newton subiteration scheme. The code is second-order accurate in time and third-order accurate in space. NXAIR includes several implicit solution algorithms and allows for grid

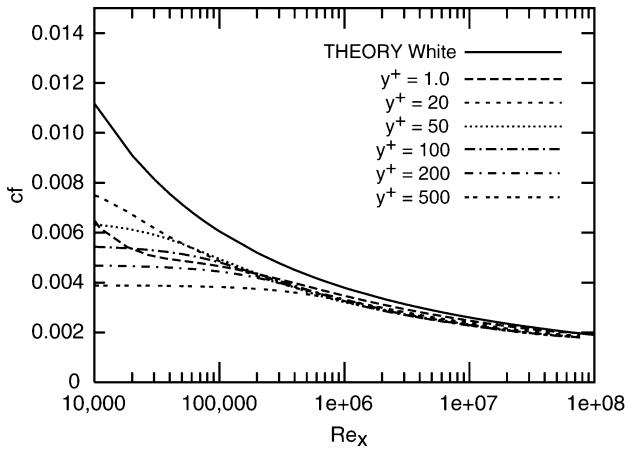

Fig. 2 Flat plate skin friction predictions for Spalart–Allmaras turbulence model with wall functions for varying initial wall grid point spacing.

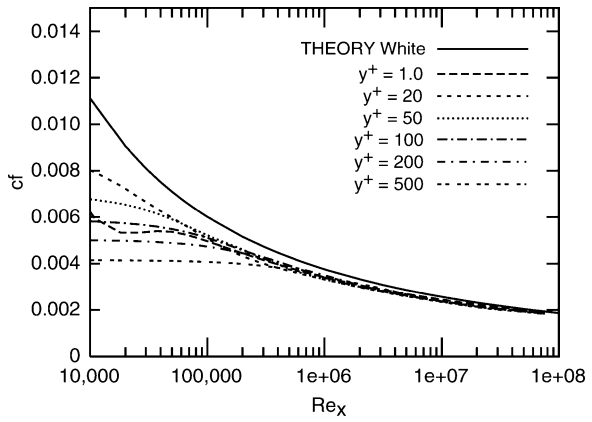

Fig. 3 Flat plate skin-friction predictions for the SST turbulence model with wall functions for varying initial wall grid point spacing.

sequencing and multigrid solution cycles. The turbulence models are solved decoupled from the mean flow equations at each Newton subiteration. The Spalart–Allmaras one-equation and the SST two-equation turbulence models contained in NXAIR were modified to include the wall function boundary conditions. The wall function boundary condition was applied explicitly, although the Newton subiteration tends to give an implicit flavor to the boundary condition implementation. The code uses automatic switching when the wall function option is selected. The wall functions currently perform the automatic switching at $y^+ = 5$.

Grid Sensitivity for a Flat Plate with Adiabatic Walls

The predicted and theoretical values for the skin-friction distribution on an adiabatic flat plate with varying initial grid wall spacings using the Spalart–Allmaras turbulence model are shown in Fig. 2 and using the SST turbulence model are shown in Fig. 3. The theoretical values are from White.[15] The $y^+ = 1$ results were not performed with wall functions and are included for reference. All of the results shown here used a grid stretching ratio of 1.2. The wall function predictions of skin friction are very similar for both turbulence models. The models are in reasonable agreement length Reynolds numbers Re_x above 1.0×10^6. Velocity profiles for the two turbulence models are shown in Figs. 4 and 5. Again the $y^+ = 1.0$ results were not run with wall functions and are included for reference. The velocity profiles are in reasonable agreement with each other and with theory for all of the wall spacings run here.

Grid Sensitivity for an Axisymmetric Bump

A second example of the grid sensitivity of the wall function boundary conditions for adiabatic walls that includes a pressure gradient is the NASA Ames Research Center transonic axisymmetric bump experiment.[16] The geometry is shown in Fig. 6. The model consisted of a sharp-lipped hollow cylinder with a 15.2-cm outer surface diameter. The bump was a circular arc 20.3 cm long and 1.9 cm high that begins 60.3 cm downstream of the cylinder leading edge. The upstream intersection of the bump and cylinder was faired with a circular arc. The test was run at a Mach number of 0.875 and a chord Reynolds number of 2.67×10^6. Surface pressure and laser velocimetery data were obtained on this configuration.

Both the Spalart–Allmaras and the SST models were run with varying initial grid wall spacings. Results for the pressure coefficient for the Spalart–Allmaras model and the SST model are shown in Figs. 7 and 8, respectively. Results for the velocity distribution at $x/c = 1.0$ (the trailing edge of the bump) are shown for the Spalart–Allmaras and the SST models in Figs. 9 and 10, respectively. The $y^+ = 1.0$ results were not run with wall functions and are included for reference. For both the pressure coefficient distribution and the velocity profile at $x/c = 1.0$, the results for each model are similar.

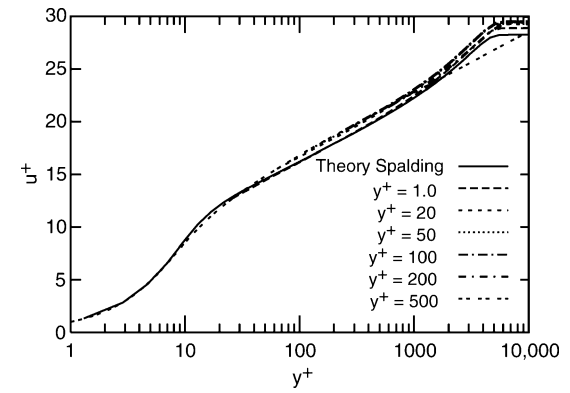

Fig. 4 Flat plate velocity profile predictions for Spalart–Allmaras turbulence model with wall functions for varying initial wall grid point spacing.

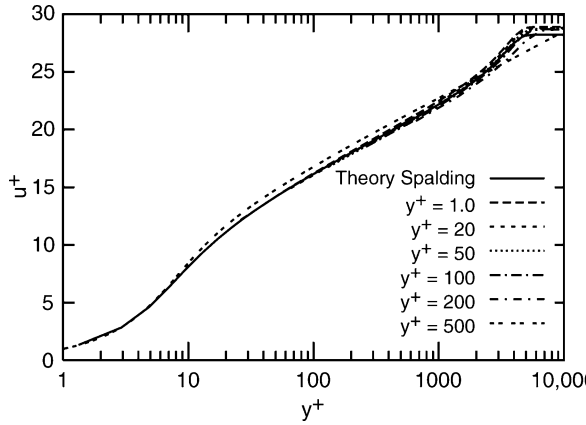

Fig. 5 Flat plate velocity profile predictions for SST turbulence model with wall functions for varying initial wall grid point spacing.

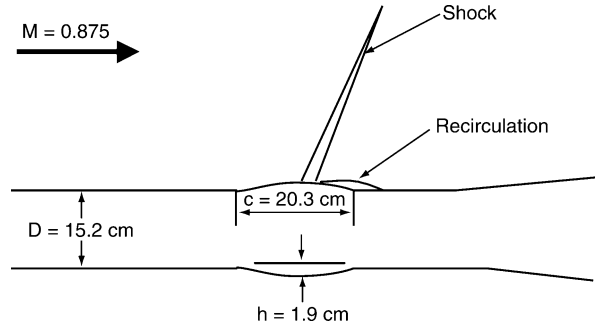

Fig. 6 Geometry for the NASA Ames Research Center axisymmetric bump experiment.

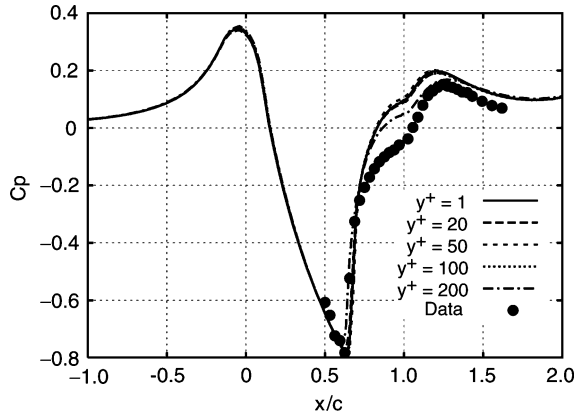

Fig. 7 Pressure coefficient predictions for NASA Ames Research Center axisymmetric bump for Spalart–Allmaras turbulence model with wall functions for varying initial wall grid point spacing.

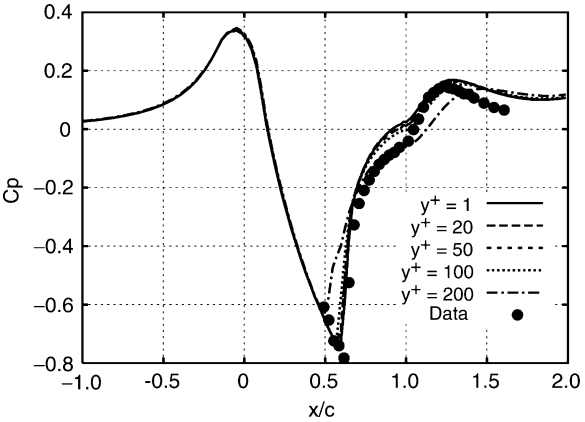

Fig. 8 Pressure coefficient predictions for NASA Ames Research Center axisymmetric bump for SST turbulence model with wall functions for varying initial wall grid point spacing.

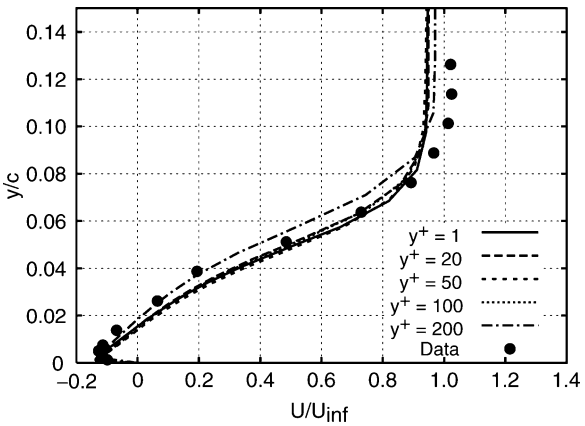

Fig. 9 Velocity distribution at $x/c = 1.0$ for NASA Ames Research Center axisymmetric bump for Spalart–Allmaras turbulence model with wall functions for varying initial wall grid point spacing.

The results tend to start to diverge for $y^+ = 200$ but are in good agreement for y^+ values of 100 or less. Note that the wall function produce reasonable results for this shock-induced boundary-layer separation.

Grid Sensitivity for a Flat Plate with Heat Transfer

Calculating heat transfer accurately can be more difficult than predicting skin friction. This can be seen in the subsonic flat plate example when the wall temperature is specified to be 1.5 times the freestream temperature. The sensitivity of the skin friction and heat

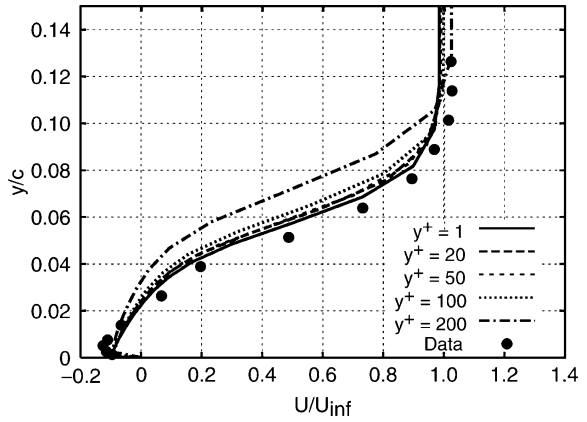

Fig. 10 Velocity distribution at $x/c = 1.0$ for NASA Ames Research Center axisymmetric bump for SST turbulence model with wall functions for varying initial wall grid point spacing.

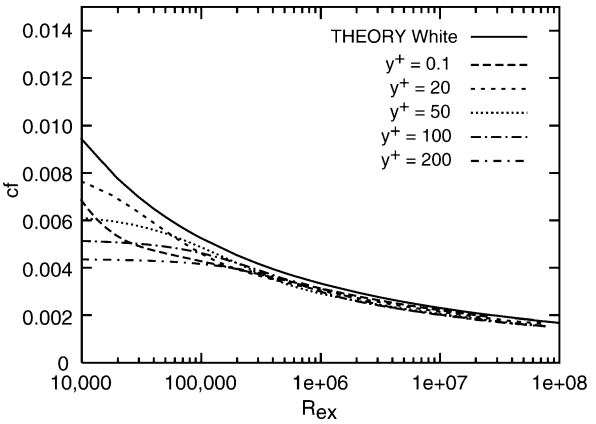

Fig. 11 Effect of wall spacing on skin friction on a flat plate with heat transfer using Spalart–Allmaras turbulence model.

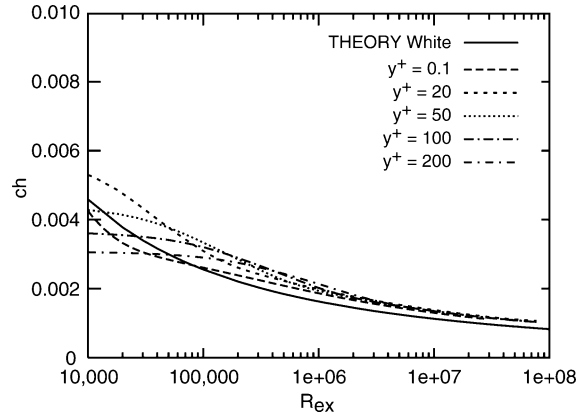

Fig. 12 Effect of wall spacing on the heat transfer (Stanton number) on a flat plate using Spalart–Allmaras turbulence model.

transfer result with varying initial grid wall spacing is shown in Figs. 11 and 12 for the Spalart–Allmaras model and in Figs. 13 and 14 for the SST model. The theoretical results are from White.[15] The $y^+ = 0.1$ results were not run with wall functions and are included for comparison. The grid stretching ratio was fixed at 1.2 for these results. Both the skin friction and heat transfer seem to be relatively insensitive to the wall spacing for the wall spacings presented here above a length Reynolds number $Re_x = 1 \times 10^6$.

Profiles of velocity and temperature at a length Reynolds number $Re_x = 1 \times 10^7$ are shown in Figs. 15 and 16, respectively, for the Spalart–Allmaras model and in Figs. 17 and 18 for the SST model. Again the $y^+ = 0.1$ results were not run with wall functions and

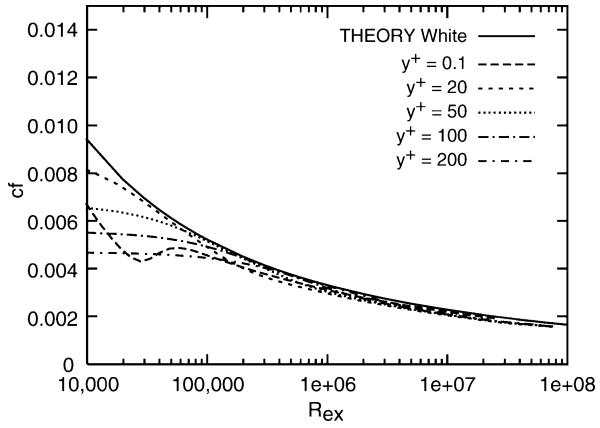

Fig. 13 Effect of wall spacing on skin friction on a flat plate with heat transfer using SST turbulence model.

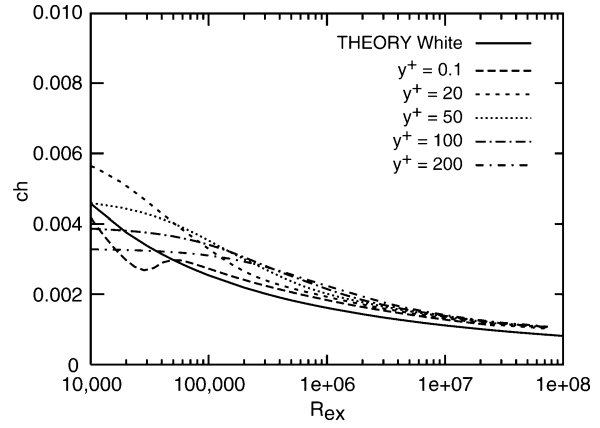

Fig. 14 Effect of wall spacing on heat transfer (Stanton number) on a flat plate using SST turbulence model.

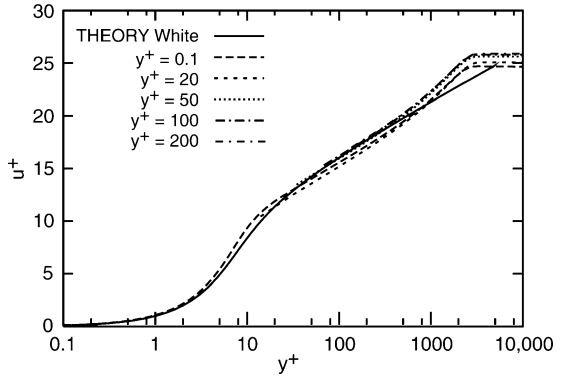

Fig. 15 Effect of wall spacing on velocity profile on a flat plate with heat transfer using Spalart–Allmaras turbulence model and wall functions.

are included for comparison purposes. The wall function results are in reasonable agreement for all wall spacings investigated for both turbulence models.

Grid Sensitivity for a Nozzle with Heat Transfer

Flow through a supersonic nozzle with a constant temperature wall can serve as a test case for evaluating the performance of the turbulence model in the presence of strong pressure gradients. Back et al.[17] measured the wall pressure distribution and heat transfer for a converging–diverging nozzle with a throat diameter of 0.0458 m and an exit diameter of 0.1227 m. High-pressure air was heated by the internal combustion of methanol and flowed along a cooled constant area duct with a length of 0.4572 m and a diameter of 0.355 m before entering the nozzle. The nozzle geometry and boundary conditions

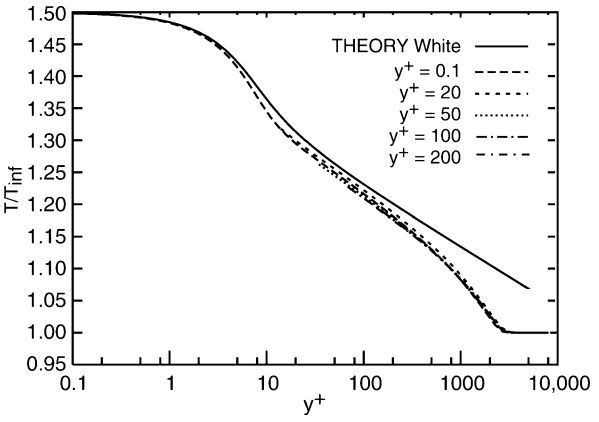

Fig. 16 Effect of wall spacing on temperature profile on a flat plate with heat transfer using Spalart–Allmaras turbulence model and wall functions.

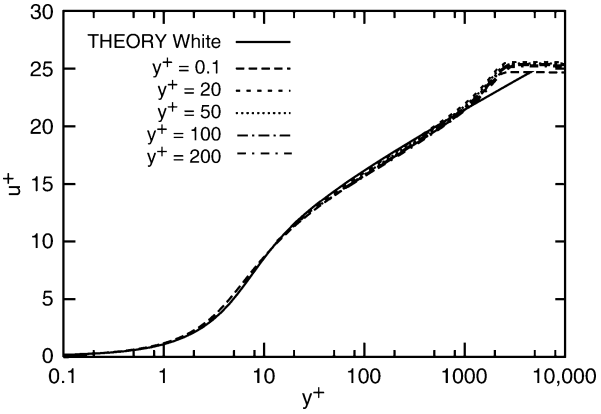

Fig. 17 Effect of wall spacing on velocity profile on a flat plate with heat transfer using the SST turbulence model and wall functions.

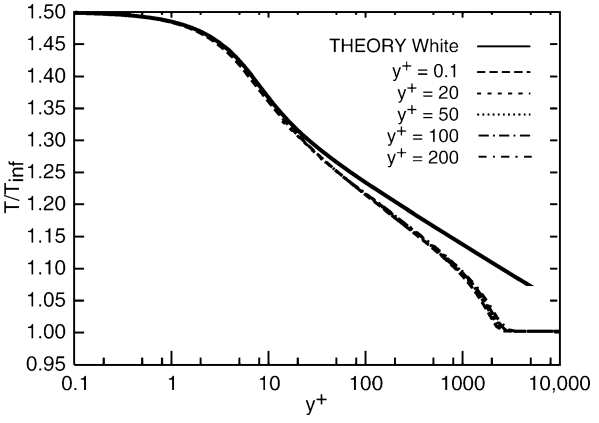

Fig. 18 Effect of wall spacing on temperature profile on a flat plate with heat transfer using the SST turbulence model and wall functions.

are shown in Fig. 19. The gas could be treated as a calorically perfect gas with a ratio-of-specific heats γ of 1.345. The nozzle exit Mach number was approximately 2.5. The molecular viscosity and thermal conductivity were assumed to vary according to Sutherland's law.

The grid-stretching ratio used in this study was 1.2. Comparisons of the predicted and measured pressure along the nozzle are shown in Fig. 20 for the Spalart–Allmaras model and in Fig. 21 for the SST model. The results for a wall spacing of $y^+ = 0.1$ were not run with wall functions and are included for reference. The pressure distribution is seen to be insensitive to the wall spacing. The wall heat transfer is shown in Fig. 22 for the Spalart–Allmaras model and in Fig. 23 for the SST model. The SST results for heat transfer are

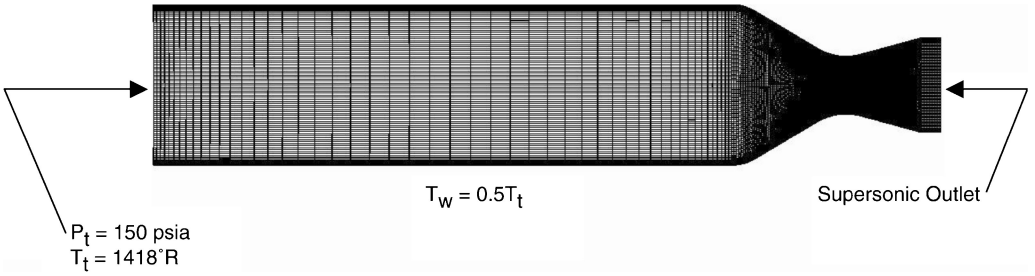

Fig. 19 Nozzle geometry.

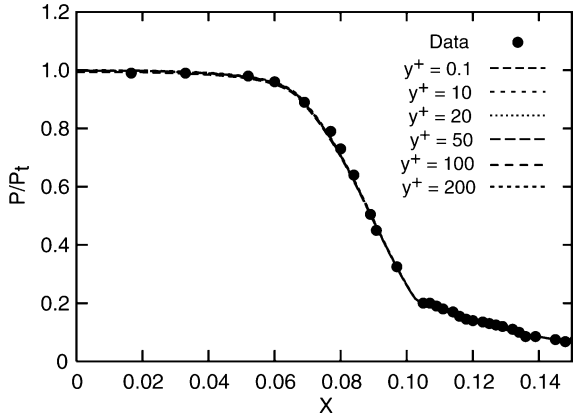

Fig. 20 Effect of wall spacing on the pressure distribution for a supersonic nozzle with heat transfer using Spalart–Allmaras turbulence model and wall functions.

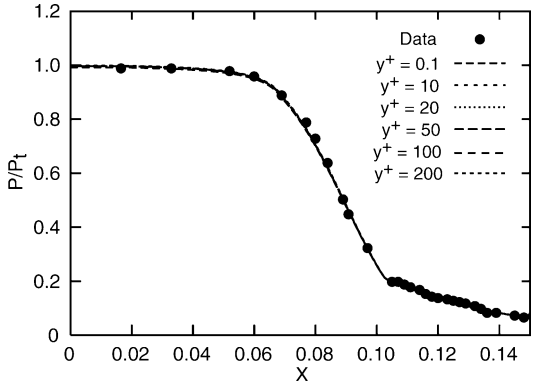

Fig. 21 Effect of wall spacing on pressure distribution for a supersonic nozzle with heat transfer using SST turbulence model and wall functions.

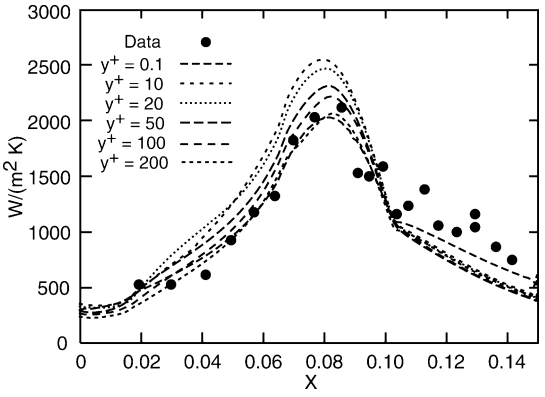

Fig. 22 Effect of wall spacing on heat transfer distribution for a supersonic nozzle with heat transfer using Spalart–Allmaras turbulence model and wall functions.

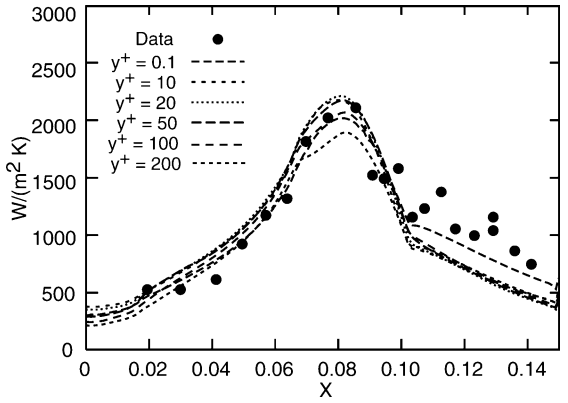

Fig. 23 Effect of wall spacing on heat transfer distribution for a supersonic nozzle with heat transfer using SST turbulence model and wall functions.

much less sensitive to the initial wall spacing than are the Spalart–Allmaras results. The heat transfer predictions are adequate for many applications even for an initial wall spacing of $y^+ = 100$ and are probably within the accuracy of the correlations used to define the wall function.

Conclusions

A general set of wall function boundary conditions has been developed and demonstrated for compressible flows with and without heat transfer at the wall. The wall functions are based on coupled profiles for velocity and temperature in the lower part of the boundary layer. The wall function boundary conditions are developed within a rigid set of assumptions so that a consistent set of relationships are developed for the wall shear stress, wall heat transfer, and the turbulence quantities at the first point off the wall. This results in wall functions that are valid in the sublayer, in the log layer, and in the transition region between these regions. The wall functions can be automatically switched on or off locally based on the local value of y^+ when they are used with in conjunction with a low-Reynolds-number turbulence model formulation.

The wall function boundary conditions were incorporated into two transport-type turbulence models. The computed results with the wall functions were in good agreement with theory and with low Reynolds number results for all of the cases attempted here for wall spacings of $y^+ \leq 100$. These larger wall spacings significantly reduce the number of points required to obtain a turbulent Navier–Stokes solution and significantly reduce the maximum Courant–Friedrichs–Lewy number for a viscous solution.

Acknowledgments

The research reported herein was performed by the Arnold Engineering Development Center (AEDC), Air Force Materiel Command. Work and analysis for this research were performed by personnel of the University of Alabama at Birmingham and by personnel of Jacobs Sverdrup AEDC Group, technical services contractor for AEDC.

References

[1]Millikan, C. B. A., "A Critical Discussion of Turbulent Flows in Channels and Circular Tubes," *Proceedings of the Fifth International Congress of Applied Mechanics*, 1938, pp. 386–392.

[2]Tennekes, H., and Lumley, J. L., *A First Course in Turbulence*, MIT Press, Cambridge, MA, 1972.

[3]Nichols, R. H., "Development and Validation of a Two-Equation Turbulence Model with Wall Functions for Compressible Flow," AIAA Paper 96-2385, July 1996.

[4]Viegas, J. R., Rubesin, M. W., and Horstman, C. C., "On the Use of Wall Functions as Boundary Conditions for Two-Dimensional Separated Compressible Flows," AIAA Paper 85-0180, Jan. 1985.

[5]Smith, B. R., "The *k–kl* Turbulence Model and Wall Layer Model for Compressible Flows," AIAA Paper 90-1483, June 1990.

[6]Wilcox, D. C., "Wall Matching, A Rational Alternative to Wall Functions," AIAA Paper 89-0611, Jan. 1989.

[7]Frink, N. T., "Assessment of an Unstructured-Grid Method for Predicting 3-D Turbulent Viscous Flows," AIAA Paper 96-0292, Jan. 1996.

[8]Spalding, D. B., "A Single Formula for the Law of the Wall," *Journal of Applied Mechanics*, Vol. 28, No. 3, 1961, pp. 444–458.

[9]Shih, T.-S., Povinelli, L. A., Liu, N.-S., Potapczuk, M. G., and Lumley, J. L., "Turbulence Surface Flow and Wall Function," AIAA Paper 99-2392, June 1999.

[10]White, F. M., and Christoph, G. H., "A Simple Analysis of Compressible Turbulent Two-Dimensional Skin Friction Under Arbitrary Conditions," U.S. Air Force Flight Dynamics Lab., AFFDL-TR-70-133, Wright–Patterson AFB, OH, Feb. 1971.

[11]Sondak, D. L., and Pletcher, R. H., "Application of Wall Functions to Generalized Nonorthogonal Curvilinear Coordinate Systems," *AIAA Journal*, Vol. 33, No. 1, 1995, pp. 33–41.

[12]Spalart, P. R., and Allmaras, S. R., "A One-Equation Turbulence Model for Aerodynamic Flows," AIAA Paper 92-0439, Jan. 1992.

[13]Veiser, W., Esch, T., and Menter, F., "Heat Transfer Predictions Using Advanced Two-Equation Turbulence Models," CFX Technical Memorandum, CFX-VAL10/0602, Waterloo, ON, Canada, Nov. 2002.

[14]Nichols, R., and Tramel, R., "Applications of a Highly Efficient Numerical Method for Overset Mesh Moving Body Problems," AIAA Paper 97-2255, June 1997.

[15]White, F. M., *Viscous Fluid Flow*, McGraw–Hill, New York, 1974, pp. 559–575.

[16]Johnson, D. A., "Predictions of Transonic Separated Flow with an Eddy-Viscosity/Reynolds Shear Stress Closure Model," AIAA Paper 85-1683, July 1985.

[17]Back, L. H., Massier, P. F., and Gier, H. L., "Convective Heat Transfer in a Convergent–Divergent Nozzle," *International Journal of Heat Mass Transfer*, Vol. 7, 1964, pp. 549–568.

P. Givi
Associate Editor